Oil & Natural Gas Technology

DOE Award No.: DE-FE0028972

Quarterly Research Performance

(Period Ending 12/31/2019)

Characterizing Baselines and Change in Gas Hydrate Systems using EM Methods

Project Period (10/01/2016 – 12/31/2019)

Submitted by:

Steven Constable

Digitally signed by Steven Constable
DN: cn=Steven Constable, o=UCSD, ou=IGPP/SIO, email=sconstable@ucsd.edu, c=US
Date: 2020.02.07 16:25:33 -08'00'

Scripps Institution of Oceanography
University of California San Diego
DUNS #: 175104595
9500 Gilman Drive
La Jolla, CA 92093-0210
Email: sconstale@ucsd.edu
Phone number: (858) 534-2409

Prepared for:
United States Department of Energy
National Energy Technology Laboratory

10/31/2017

U.S. DEPARTMENT OF ENERGY | NATIONAL ENERGY TECHNOLOGY LABORATORY

Office of Fossil Energy

TABLE OF CONTENTS

Page

EXECUTIVE SUMMARY

This review period was occupied by writing project results up for publication in *Geophysical Research Letters* (one manuscript) and *The Fire in the Ice* (two manuscripts). The drafts of these three papers are presented in this final quarterly report.

ACCOMPLISHMENTS

Major goals of project

Methane hydrates require cool temperatures, high pressures, and methane in excess of solubility to form, conditions that are met in both marine and permafrost regions worldwide. Concentrated accumulations of structural hydrate may be the target for resource exploitation, and there have been several production tests of natural gas from hydrate, both on land, such as at the Mallik site in NW Canada or the Mt Elbert test well on the Alaska North Slope, and in the ocean, such as in the Nankai Trough and an ice platform off Prudhoe Bay.

Much naturally occurring hydrate exists at the edge of thermodynamic stability, and as such represents an environmental hazard that threatens release of a potent greenhouse gas as a consequence of warming. Also, one way to produce methane from hydrate is to destabilize the structure by depressurization.

Current geophysical surveying methods for identifying hydrates, such as seismic methods and well logging/coring, are limited. Quantifying the volume fraction of hydrate in sediments is possible with careful processing and inversion of seismic data, although the relationship between seismic velocity (or attenuation) and hydrate concentration is complicated and usually needs to be calibrated with well data. Electromagnetic (EM) methods, on the other hand, are sensitive to the concentration and geometric distribution of hydrate because regions containing hydrate are significantly more resistive when compared to water saturated zones. The current state of the art for imaging gas hydrate using EM methods is represented by the Vulcan system developed by Scripps Institution of Oceanography. This system uses multiple, 3-axis EM receivers towed at source-receiver ranges of up to 1,000 m behind an electric dipole transmitter. The whole array (transmitter and receivers) is "flown" 50–100 m above the seafloor in order to (a) reduce noise, (b) avoid seafloor infrastructure and other obstacles, and (c) allow all three components of electric field to be measured. The Vulcan system was used in 2014 and 2015 to successfully collect 1,000 km of high quality data over gas hydrate prospects in Japan, as well as two studies offshore San Diego, California.

For the next advance in this technology, under the current agreement we will collect extensive 3D Vulcan data sets over two or three sites in the Gulf of Mexico where drilling and coring of hydrate systems has been, or will be, carried out. We plan to study the Walker Ridge 313, Orca Basin, and Green Canyon 781 prospects, but as we did under previous NETL funding, we will consult with DoE and the drilling consortium before choosing final targets. With 2–3 days of data collection over each prospect, we will be able to collect at least 10 lines of data 10–20 km long. With a line spacing of 500–1,000 m, this will provide a dense data set of 100–200 line km covering 50–100 square km.

Under prior NETL funding we designed a specialty pressure cell plumbed for high-pressure gas access, in which we formed gas hydrate samples while simultaneously measuring impedance spectra. Such impedance measurements of methane hydrate are needed for modeling of gas hydrate systems, yet had never been established prior to our work. Under the current agreement, we plan to extend these laboratory experiments to further utilize the unique apparatus we have designed, and build on our previous results and baseline measurements. We will introduce additional parameters that mimic the effects of induced or environmental factors that may act to destabilize gas hydrate systems and contribute to the onset of partial dissociation to solid or liquid water.

Work accomplished during the project period

During the project period we wrote three manuscripts, two of which have been submitted to *The Fire in the Ice* and one about to be submitted to *Geophysical Research Letters*.

Manuscript for submission to Geophysical Research Letters

Laboratory Electrical Conductivity of Marine Gas Hydrate

Steven Constable, Ryan Lu, Laura A. Stern, Wyatt L. Du Frane, John C. Pinkston, Jeffery J. Roberts

Abstract

Methane hydrate was synthesized from pure water ice and flash frozen seawater, with varying amounts of sand and silt added. Electrical impedance spectroscopy was used to measure the electrical conductivity of the samples, using equivalent circuit modeling to separate the effects of electrodes from the samples and to gain insight into the electrical conduction mechanisms. Silt and sand increase the electrical conductivity of pure methane hydrate, inferred to be a result of contaminant NaCl contributing to electrical conduction in hydrate, to a peak conductivity which is in agreement with peak resistivities observed in well logs through massive hydrate (3,000–10,000 Ωm). The addition of silt and sand lowers the electrical conductivity of methane hydrate synthesized from seawater, by an amount that is consistent with a simple application of Archie's Law. All samples were characterized using cryogenic scanning electron microscopy and energy dispersive spectroscopy after quenching in liquid nitrogen, which shows good connectivity of salt and brine phases. Electrical conductivity measurements of pure hydrate and hydrate mixed with silt during pressure-induced dissociation supports previous conclusions that the presence of sediment increases dissociation rate.

Introduction

Gas hydrate is a solid compound of water ice and gas, usually methane (CH_4), that forms at temperatures and pressures found on the continental shelves deeper than about 500 m. Although vast amounts of carbon are sequestered as hydrate, 1,000 to 100,000 Gt globally, this total is uncertain [Milkov, 2004]. The majority of hydrate is dispersed at low concentrations [Boswell and Collett, 2011], but some marine gas hydrate forms in high concentrations as pore-filling material in clastic sediments such as sands and silts. Such deposits are of interest as a supply of natural gas, particularly for countries that lack conventional hydrocarbons, and several offshore production tests have been made [Fujii et al., 2015; Yamamoto et al., 2014]. Dissociation of gas hydrate situated at the edge of its stability field has been implicated in seafloor landslides [e.g. Nixon and Grozic, 2007; Paull et al., 2008] which may potentially generate tsunamis. Rapid release of methane to seawater could contribute to ocean acidification [Biastoch et al., 2011], and even climate change if methane reaches the atmosphere in shallow arctic waters [Wadhams, 2016].

Much of our understanding of seafloor gas hydrate comes from seismic surveys and drilling, either as by-products of conventional hydrocarbon exploration of as targeted scientific studies. These methods are both expensive and subject to limitations. The seismic method is blind to low hydrate concentrations, and even high concentrations are difficult to identify and quantify without control from well logs. Drilling provides a good understanding of seafloor geology, but hydrate rapidly changes concentration in a lateral direction, so data along one vertical profile cannot easily be extrapolated.

Gas hydrate is electrically resistive, a feature that is exploited in well logging [e.g. Collett and Lee, 2011], and can be imaged using marine controlled-source electromagnetic (CSEM) methods [e.g. Weitemeyer et al., 2006; Schwalenberg et al., 2010; Constable et al., 2016; Wang et al., 2017]. To assist in the interpretation of CSEM data, in a series of previous papers we investigated electrical conductivity as a function of temperature for pure methane hydrate [Du Frane et al., 2011], hydrate with sand [Du Frane et al., 2015], and hydrate with salt (NaCl) [Lu et al., 2019]. Here we conclude these studies by comparing the effect of sand and silt with hydrate synthesized from pure water and flash-frozen seawater, and examining conductivity during pressure-induced dissociation. Combined with the previous studies, our results provide a comprehensive picture of methane hydrate conductivity. Sediments contribute to the conductivity of methane hydrate, silt more than sand when mixed at the same volume percent. We infer the charge carriers to be associated with sodium and/or chlorine ions, since the activation energy with temperature is similar to samples with NaCl added. Samples with hydrate synthesized from flash frozen seawater are 1–2 orders of magnitude more conductive, presumably because of connected brine. The simplest version of Archie's Law with an exponent of 2 predicts the conductivity of samples synthesized with 50% sediment and seawater.

Sample preparation

Samples were prepared from granular "seed" ice + CH_4 gas $\pm$ SiO_2 (sand or silt) reactants to produce polycrystalline methane hydrate both with and without a sediment component, using the thermal-cycling method developed by Stern et al. [1996, 2004] and modified for the current work as described by Du Frane et al. [2011, 2015] and Lu et al. [2019]. Seed ice was prepared from either triple-distilled water or synthetic seawater containing 3.5wt% salts that was flash frozen in liquid nitrogen [Lu et al., 2019]. For two samples here, pure H_2O seed ice was pre-mixed with silica silt to produce final samples containing 10 vol% and 50 vol% silt, respectively, relative to the methane hydrate component (Table 1; NH+Silt10 and NH+Silt50). A third sample was prepared with 50 vol% silt mixed with seawater ice (Table 1; SH+Silt50), and a fourth from 50 vol% quartz sand mixed with seawater ice (Table 1; SH+Sand50). Silt used here was Min-U-Sil40 supplied by U.S. Silica, with >99.5% purity SiO_2 and 10.5μm average particle size. Sand was Oklahoma #1, >99% purity SiO_2 with 84% grain-size distribution of 106–0.250 μm, also used in Du Frane et al. [2015]. In addition to the four samples described above, Table 1 lists six previous experiments from Du Frane et al. [2015] and Lu et al. [2019] relevant to the current work and discussion. The sample naming convention is NH for hydrate synthesized from high purity ice, and SH for hydrate synthesized from seawater, followed by the added product (silt, sand, or NaCl) and the percentage by weight or volume.

Table 1. Methane hydrate synthesis conditions, conductivity at +5°C, and Arrhenius fits.

Sample Name	Sample Conditions	σ(S/m) at +5°C	Ea (kJ/mol)	log(σ_o)
NH*	CH_4 hydrate synthesized from ice	3.49E-05	33.62	1.861
NH+NaCl0.25*	CH_4 hydrate from ice with 0.25wt% NaCl	2.85E-04	36.62	3.362
NH+NaCl1.0*	CH_4 hydrate from ice with 1.0wt% NaCl	1.31E-03	35.52	3.281
NH+Sand10†	CH_4 hydrate from ice with 10vol% Sand	7.80E-05	31.31	1.779
NH+Sand45†	CH_4 hydrate from ice with 45vol% Sand	9.98E-05	43.18	4.122
NH+Silt10	CH_4 hydrate from ice with 10vol% Silt	1.50E-04	30.58	1.973
NH+Silt50	CH_4 hydrate from ice with 50vol% Silt	2.03E-04	37.82	3.442
SH*	CH_4 hydrate synthesized from frozen seawater	3.02E-01	86.38	15.58
SH+Sand50	CH_4 hydrate from seawater with 50vol% Sand	6.40E-02	76.11	13.12
SH+Silt50	CH_4 hydrate from seawater with 50vol% Silt	3.63E-02	80.26	13.67

†Sample data from Du Frane et al. 2015
*Sample data from Lu et al. 2019

All experiments were conducted in a custom pressure vessel in which gas hydrate is synthesized while simultaneously collecting in situ impedance (Z) spectroscopy measurements [Du Frane et al., 2011]. Initial porosity for all samples was 36 vol% prior to reaction, and the resulting material is a methane hydrate + sediment aggregate with ≈25% porosity [Lu et al., 2019]. In samples formed from seawater ice, a liquid brine component also develops [Lu et al., 2019].

Each sample underwent at least 6 thermal cycles during synthesis, until electrical impedance stopped changing significantly between cycles. A final incremental "step-dwell" heating cycle involved a 1-hour hold at each target temperature to allow thermal equilibration of the sample before making electrical impedance measurements. With the exception of sample NH+Silt50, all samples were then quenched in liquid nitrogen for post-run analysis (described below).

Following step-dwell impedance measurements on sample NH+Silt50, this sample was partially dissociated to generate H_2O pore water within it to monitor impedance changes relative to the sample's original fluid-free state, and to compare with those samples formed from seawater ice that developed a liquid brine component. Sample NH+Silt50 was depressurized across the methane hydrate phase stability boundary while holding external temperature at +5°C, forcing it to partially dissociate to water + gas in a relatively uniform manner [Lu et al., 2019]. Pressure was slowly released from 20 MPa to 5 MPa, allowing sufficient time for sample equilibration following isochoric cooling effects, was then reduced again to 3.8 MPa, 0.6 MPa below the equilibrium boundary, to induce partial dissociation of the

methane hydrate and in situ pore water production. After 45 minutes, the sample was quenched in liquid nitrogen.

All samples in the present study were recovered for analysis of phase distribution and grain-scale characteristics by cryogenic scanning electron microscopy (cryo-SEM) and energy dispersive spectroscopy (EDS) methods [Stern et al., 2004; Lu et al., 2019]. Imaging was conducted at <-185°C, 10-15 kV, in low-vacuum mode with chamber pressure of $\approx$ 20 Pa. Representative images are shown in Figure 1.

Cryo-SEM and EDS

Figure 1 shows cryo-SEM images and EDS measurements from four samples, all containing sediment. Ice-derived methane hydrate with 10% silt (Figure 1a) exhibits dense regions of methane hydrate (smooth, darker regions) surrounded by individual grains or small clusters of silt (small, brighter particles). The identification of methane hydrate and silt is verified by the presence of carbon and silica peaks, respectively, in EDS spot measurements (blue insets). The run of ice-derived methane hydrate with 50% silt (Figure 1b) was extensively dissociated prior to quenching, and the EDS measurements show that minimal carbon remains. In the run containing 50% silt and hydrate synthesized from seawater (Figure 1c), silty regions cluster locally but are well distributed at the sample-wide scale. Here hydrate often appears rounded or botryoidal where remaining briny fluid crystallizes or "freezes" on or proximal to it, as exposed along open cavities. EDS measurements show that NaCl-bearing phase(s) also concentrate in silty regions. Figure 1d shows a similar seawater-derived sample where the silt is replaced by 50% sand, with a similar appearance apart from less clumping of the sediment. The SEM image is matched with EDS elemental maps of O (Figure d1), which corresponds to both hydrate and sand; Si (Figure d2), which corresponds to sand; C (Figure d3), which maps hydrate location; and Na (Figure d4), which delineates NaCl. While not quantitative, the EDS maps show the general distribution of these components in the SEM image. The shading is a result of the low angle of the incident radiation. The overall good distribution and connectivity of frozen brine and/or salt phases is indicated by the Na map. Additional SEM images of methane hydrate $\pm$ quartz sand $\pm$ NaCl-bearing phases, including hydrate formed from seawater-ice, are shown in Lu et al. [2019].

Electrical Characterization

For each run and each temperature, complex electrical impedance was measured at 27 frequencies between 0.5 kHz and 300 kHz, as described in Lu et al. [2019], and plotted as "Cole-Cole" plots in the complex plane. Figure 2 shows examples of such plots at representative temperatures for four runs considered here. Such impedance spectroscopy is necessary to separate the effect of charge polarization at the silver electrodes and the resistance/capacitance of the actual sample [e.g. Roberts and Tyburczy, 1994; 1999]. In the studies of Du Frane et al. [2011, 2015], which examined simple systems of pure methane hydrate and hydrate with sand or glass beads (plus about 25% CH_4 gas), electrical conductivity was calculated from the impedance with the smallest angle from the real axis. For the more complicated methane hydrate - NaCl brine - halite/hydrohalite systems studied by Lu et al. [2019], equivalent circuit modeling (ECM) was required to model sample impedance. In ECM modeling, complex impedance data are typically fit by a series of pairs of resistors (R) and capacitors (C) in parallel. A single such RC circuit generates a semicircular arc in the complex plane extending from the origin and with the center of the arc on the real axis. Here we used the ECM software of Bondarenko [2013]. Besides allowing the separation of electrode impedance, ECM also provides insight into conduction mechanisms [e.g. Lu et al., 2019].

Methane hydrate synthesized from pure ice (NH) is characterized by two RC circuits, the left-most (highest frequency) arc associated with the resistance and capacitance of the dielectric hydrate sample, and the right-most (low frequency) arc associated with electrode polarization. In ECM, if the center of the impedance arc falls below the real axis, the capacitor element needs to be replaced with a constant phase element (CPE). There are various physical reasons for this, which include an imperfect (dispersive) dielectric, an electro-chemical double-layer formed from ions adsorbed onto grain surfaces, and rough or porous electrodes. A CPE is needed to model NH sample conductivity at the warmest temperatures, which we interpret as an imperfect dielectric.

For methane hydrate synthesized from seawater (SH), the Cole-Cole plots are dominated by electrode polarization, which requires a CPE, possibly to account for roughness or lack of uniform contact. The sample part of the model

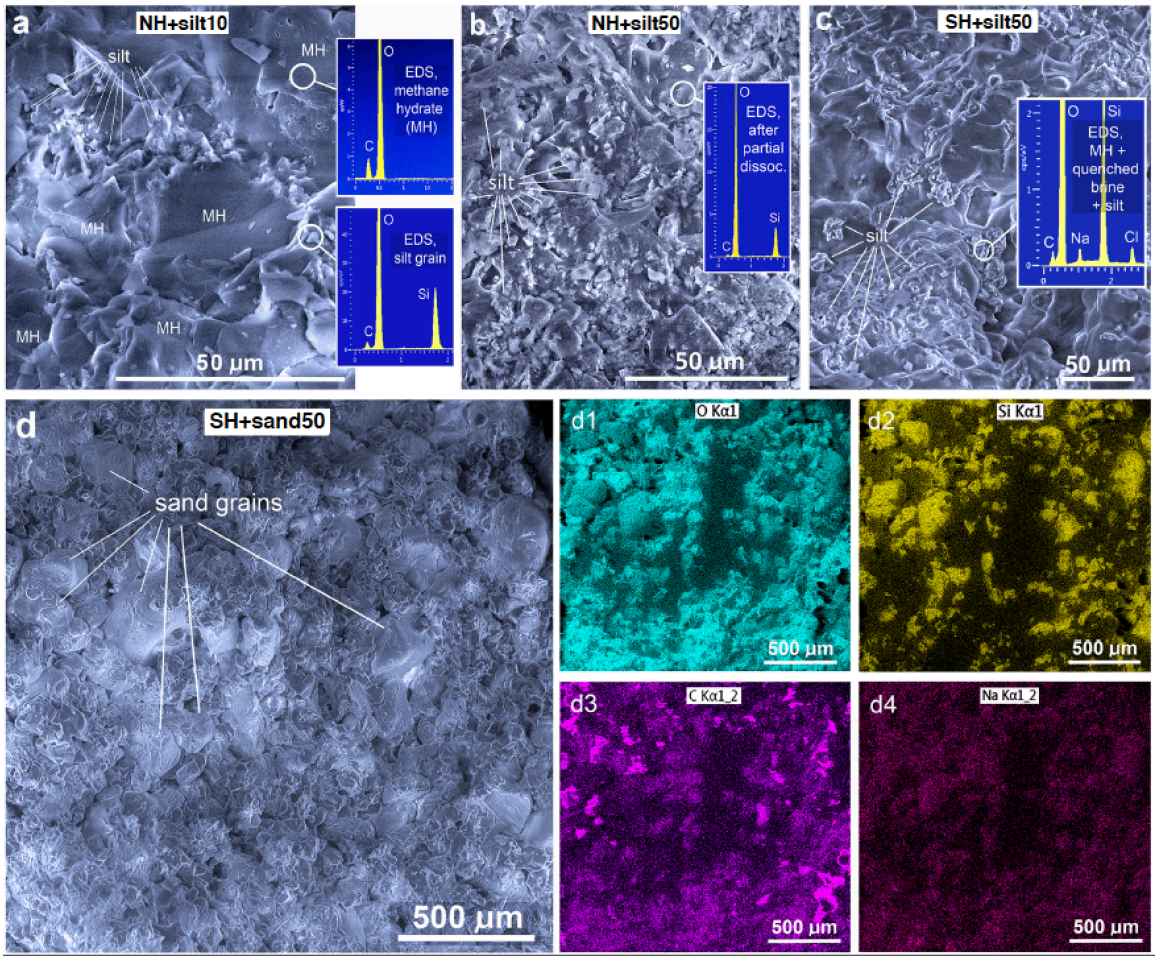

Figure 1. Cryo-SEM images and EDS measurements from methane hydrate plus sediment (sand and silt). Methane hydrate made from H_2O ice, plus (a) 10 vol% silt and (b) 50 vol% silt,. Methane hydrate made from seawater-ice and (c) 50 vol% silt and (d) 50 vol% sand. Insets d1 to d4 show EDS maps for oxygen, silicon, carbon, and sodium that correspond to the SEM image shown in (d). See text for further descriptions.

lacks a capacitive element, presumably because conductivity is dominated by a connected brine phase [Lu et al., 2019]. There is little change in impedance with temperature.

Methane hydrate synthesized from seawater ice and in the presence of sand and silt look similar to SH at warm temperature, but as the sample conductivity drops at colder temperatures, the sample begins to dominate the impedance of the sample+electrode measurement and we begin to resolve a capacitive (actually CP) element in the sample. The effect is greater for silt than sand, suggesting a relationship with surface area, and possibly that there might be an electro-chemical double-layer forming.

The resistance of the sample part of the ECM is combined with the geometry of the sample to compute electrical conductivity, which is proportional to the product of the number of charge carriers and the mobility of the charge carriers. Both the carrier density and mobility are thermally activated and described by a Boltzmann relationship, and so conductivity σ for a single charge carrier as a function of temperature is given by

$$\sigma = \sigma_o e^{-A/kT} = \sigma_o e^{-E_a/RT}$$

where k is Boltzmann's constant (1.381×10^{-23} J/K), R is the gas constant (8.314 J/mol/K), T is absolute temperature, and σ_o is a pre-exponential constant. The A and E_a are both activation energies, in electron volts and kJ/mol

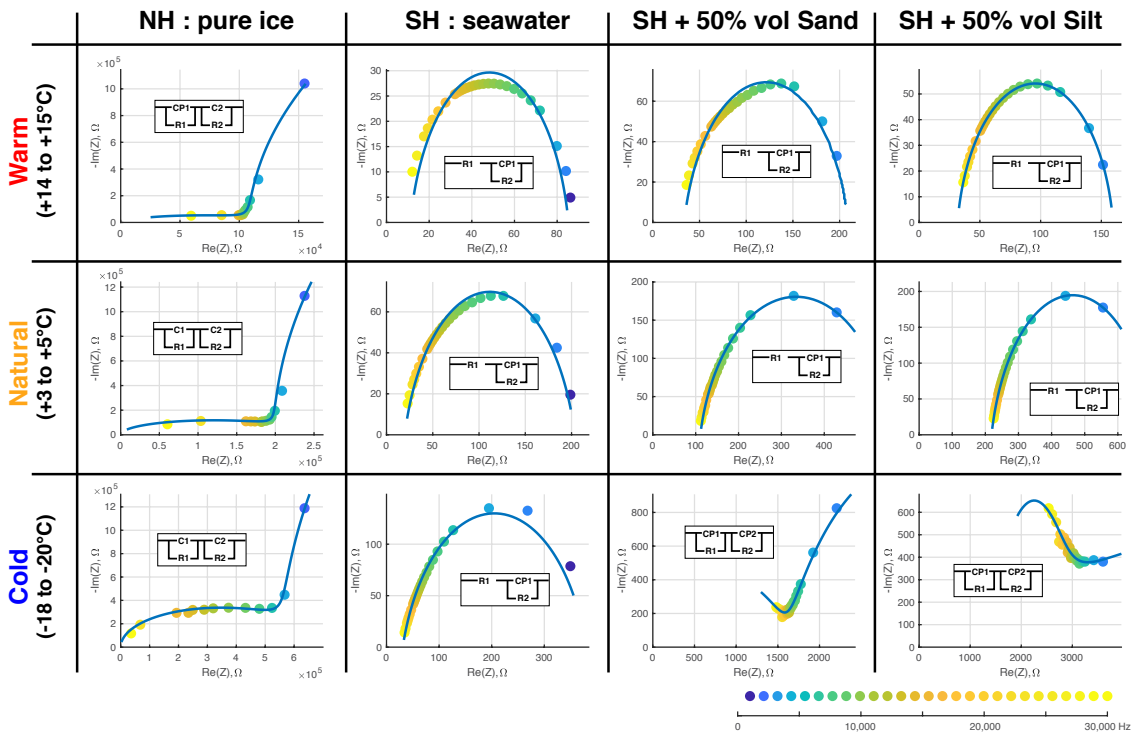

Figure 2. Equivalent Circuit Models (ECM) and fits of Cole-Cole plots at different temperatures for pure methane hydrate with 0% NaCl (NH) and three methane hydrate samples synthesized from frozen seawater. Frequency = 5k-300 kHz. R = resistor; CP = constant phase element, C = capacitor.

respectively. Here we shall use the latter. This is the Arrhenius equation, which can be linearized by plotting the logarithm of σ versus $1/T$ to create an Arrhenius plot, the slope of which gives E_a. Figure 3 presents an Arrhenius plot for the samples introduced in this paper, along with the salt-bearing samples NH, NH+NaCl0.25, NH+NaCl1.0 from Lu et al. [2019] and the sand-bearing samples NH+Sand10 and NH+Sand45 from Du Frane et al. [2015] for comparison. Du Frane et al. [2015] did not carry out ECM modeling on NH+Sand45. Here we were able to conduct ECM modeling of the original data at temperatures above -1°C, resulting in lower conductivities and activation energy.

Results

The electrical conductivity of NH+Silt10 and NH+Silt50, methane hydrate made from pure ice with added silt, is essentially the same for both samples in spite of the different proportion of sediments (10% versus 50%). Having re-computed the conductivities for NH+Sand45, the same is true of the corresponding sand samples, although the sand conductivities are about a factor of two lower than the silt. For both silt and sand, the activation energy is slightly higher for the samples with greater sediment content, but this difference is close to what we can resolve. For all four samples, the activation energy (31 to 43 kJ/mol) is similar to the sample prepared with 0.25% NaCl (37 kJ/mol), so we infer that the charge carriers are derived from NaCl. Indeed, the activation energy for hydrate synthesized from "pure" ice is also similar, 34 kJ/mol, as noted by Lu et al. [2019], again suggesting that contaminant NaCl provides the dominant charge carrier. A sample with methane hydrate in mixture with glass beads had high concentrations of Na_2CO_3 present, but little enhancement of electrical conductivity over methane hydrate by itself [Du Frane et al. 2015]. This suggests the presence of chlorine ions may play a bigger role in hydrate conductivity than sodium.

Silt samples are more conductive than sand samples, even though tests of rinse water show that sand provides more salt than the silt, per unit volume. This suggests that it is surface area, rather than available NaCl, that determines hydrate conductivity. There is a limit to the amount of NaCl that hydrate can incorporate, because below the liquidus (0°C), the conductivity of the 1% and 0.25% NaCl samples is essentially the same. It is unlikely that hydrate incorporates

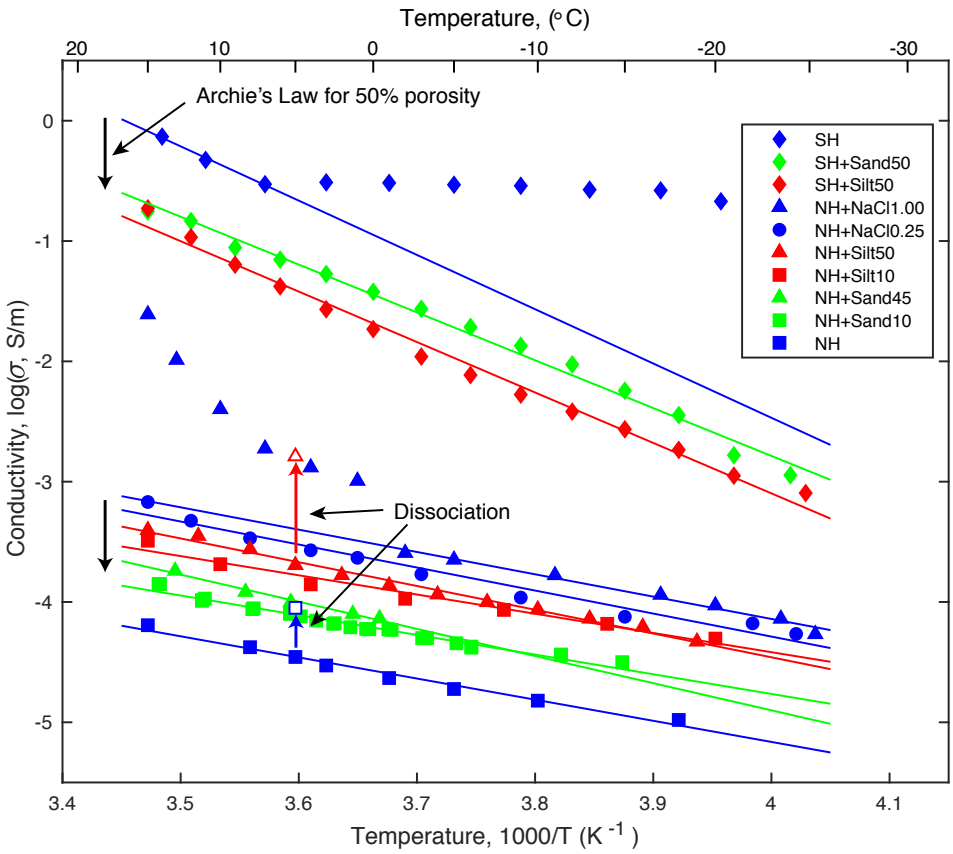

Figure 3. Conductivity versus reciprocal temperature (Arrhenius) plot for all samples. Blue symbols represent methane hydrate with no sediment, but with between 0 to 1.0 wt% NaCl (see legend box). Green symbols represent samples with sand. Red symbols represent samples with silt. Samples synthesized from seawater are shown as diamonds. Colored lines are activation energy fits as given in Table 1. Colored arrows indicate the change in conductivity after 45-minutes of partial dissociation to generate pore water. Vertical black arrows indicates the expected loss of conductivity given by Archie's Law and 50% porosity.

0.25% NaCl. Rinse water conductivity from 10% silt suggests that 0.01% NaCl is available to the hydrate. Du Frane et al. [2015] report that hydrate synthesized from seed ice had about 5×10^{-3}% contaminant NaCl. Factoring these by conductivity differences we infer that between 0.02 and 0.05% NaCl contributes to the conductivity of pure methane hydrate. The silts used in this study were primarily silica, and the effects of silt containing clays on electrical conductivity are likely more complicated.

Samples with 50% sand and silt with hydrate synthesized from flash frozen seawater (SH+Sand50 and SH+Silt50) exhibit similar activation energies (76.1 and 80.2 kJ/mol) which are higher than for the hydrate from H_2O ice, along with higher conductivities. The sand sample is about a factor of 2 higher conductivity than the silt sample. The conductivity of the seawater sample without sediment (SH) is generally independent of temperature, which Lu et al. [2019] interpreted as a fully interconnected brine network. However, we note that the three highest temperature data points for this sample have an activation energy similar to the silt/sand samples (86.4 kJ/mol), suggesting that the conductivity of the sand/silt samples is determined by brine released during hydrate formation. That the conductivity of the sand/silt samples does not become temperature independent suggests that sediment inhibits the full interconnection of brine, perhaps through capillary forces. A simple Archie's Law calculation, $\sigma = \sigma_o\Phi^2$, where Φ is porosity and here equal to 0.5, σ is the conductivity of the sediment, and σ_o is the conductivity of the brine/hydrate system, correctly predicts the conductivity of the sediment samples from the high-temperature SH data, supporting the proposal that the conduction mechanism is similar in the three samples.

Sample NH+Silt50 was partially dissociated in a similar pressure-drop manner to the way sample NH was dissociated by Lu et al. [2019]. The electrical conductivity of both samples 45 minutes after dissociation is plotted on Figure 3 for direct comparison. The dissociation rate was faster for the sediment sample, which is consistent with the observations of Circone et al. [2004], who measured faster dissociation rates in methane hydrate containing either homogeneously-mixed or inter-layered quartz sand, compared to pure methane hydrate. The quartz sand in that study was the same OK#1 used here.

Discussion and Conclusions

The similarity in conductivity for hydrate-from-ice samples with 10% and 50% sediment fractions suggests that the reduction in the conductive phase (hydrate) in the 50% samples is compensated for by an increased availability of charge carriers from the increased amount of sediment. That the silt samples are more conductive than sand samples suggests that the surface area of the sediment is the defining parameter. In the marine environment the availability of salt is not restricted by sediment, and so in an open system where brine can be excluded during hydrate formation, pure hydrate would be expected to have a conductivity similar to that of NH+NaCl0.25. The NH+Sand45 sample is consistent with NH+NaCl0.25 conductivity and Archie's Law, but the NH+Silt50 sample is more conductive than predicted by Archie's Law. This suggests that silt enhances conductivity in some way, perhaps by distributing charge carriers though hydrate more efficiently than by adding sand. In any case, we can conclude that in natural systems where brine has been excluded during hydrate formation, electrical resistivity of hydrate saturated sediment at seafloor temperatures could be as high as 3,000–10,000 Ωm, depending on grain size. Matsumoto et al. [2017] observed peak resistivities this high in logging-while-drilling data from hydrate chimneys off eastern Japan.

Samples synthesized using seawater represent the opposite extreme of a closed system where brine formed during hydrate formation remains in the sediment. Here the resistivity at seafloor temperatures is about 20 Ωm for samples with 50% sediment. While it is difficult to imagine large deposits of hydrate formed in this manner, it is possible that pockets, or thin layers, of brine-enriched hydrate might develop in association with more resistive hydrate deposits. Indeed, we have observed large electrical anisotropy in hydrate, with horizontal resistivities 20 times smaller than vertical resistivities [Constable et. al, 2020].

Acknowledgements

This work was supported by the US Department of Energy award DE-FE0028972 and DoE-USGS Interagency Agreement DE-FE0026382. Prepared by LLNL under Contract DE-AC52-07NA27344.

References:

Biastoch, A., T. Treude, L. H. Rpke, U. Riebesell, C. Roth, E. B. Burwicz, W. Park, M. Latif, C. W. BŽning, G. Madec, K. Wallmann, 2011. Rising Arctic Ocean temperatures cause gas hydrate destabilization and ocean acidification. *Geophysical Research Letters*, **38**, L08602, doi:10.1029/2011GL047222.

Boswell, R., and T.S. Collett, 2011. Current perspectives on gas hydrate resources. *Energy & Environmental Science*, **4**, 1206–1215.

Circone, S., L.A. Stern, and S.H. Kirby, 2004. The effect of elevated methane pressure on methane hydrate dissociation. *American Mineralogist*, **89**, 1192–1201.

Collett, T. S., and M.W. Lee, 2011. Downhole well log characterization of gas hydrates in nature: A review. Contributed paper at *Proceedings of the 7th International Conference on Gas Hydrates*, .

Constable, S., P. K. Kannberg, and K. Weitemeyer, 2016. Vulcan: A deeptowed CSEM receiver. *Geochemistry, Geophysics, Geosystems*, **17**, 1042–1064, doi:10.1002/ 2015GC006174.

Constable, S., R. Lu, P. Kannberg, L. Stern, W. Du Frane, and J. Roberts, 2020. In-situ and laboratory evidence for

high electrical anisotropy in marine gas hydrate. *Fire in the Ice, Methane Hydrate Newsletter, National Energy Technology Laboratory*, submitted.

Du Frane, W.L., L.A. Stern, K.A. Weitemeyer, S. Constable, J.C. Pinkston, J.J. Roberts, 2011. Electrical properties of polycrystalline methane hydrate. *Geophysical Research Letters*, **38**, doi:10.1029/2011GL047243.

Du Frane, W., L.A. Stern, S. Constable, K.A. Weitemeyer, M.M. Smith, and J.J. Roberts, 2015. Electrical properties of methane hydrate + sediment mixtures. *Journal of Geophysical Research*, **120**, 4773–4787, doi:10.1002/2015JB011940.

Fujii, T., Suzuki, K., Takayama, T., Tamaki, M., Komatsu, Y., Konno, Y., Yoneda, J., Yamamoto, K., and Nagao, J., 2015. Geological setting and characterization of a methane hydrate reservoir distributed at the first offshore production test site on the Daini?Atsumi Knoll in the eastern Nankai Trough, Japan. *Marine and Petroleum Geology*, **66**, 310–322, https://doi.org/10.1016/j.marpetgeo.2015.02.037.

Lu, R., L.A. Stern, W.L. Du Frane, J.C. Pinkston, J.J. Roberts, and S. Constable, 2019. The effect of brine on the electrical properties of methane hydrate. *Journal of Geophysical Research: Solid Earth*, **124**, 10,877–10,892.

Matsumoto, R., Tanahashi, M., Kakuwa, Y., Snyder, G., Ohkawa, S., Tomaru, H., and Morita, S., 2017. Recovery of thick deposits of massive gas hydrates from gas chimney structures, eastern margin of Japan Sea: Japan Sea Shallow Gas Hydrate Project. *Fire in the Ice, Methane Hydrate Newsletter, National Energy Technology Laboratory*, **17**, 1–6.

Milkov, A.V., 2004. Global estimates of hydrate bound gas in marine sediments: how much is really out there?. *Earth Science Reviews*, **66**, 183–197.

Nixon, M. F., and J. L. H. Grozic, 2007. Submarine slope failure due to gas hydrate dissociation: A preliminary quantification. *Canadian Geotechnical Journal*, **44**, 314–325, doi:10.1139/T06-121.

Paull, C.K., Ussler, W., Holbrook, W.S., Hill, T.M., Keaten, R., Mienert, J., Haflidason, H., Johnson, J.E., Winters, W.J., and Lorenson, T.D., 2008. Origin of pockmarks and chimney structures on the flanks of the Storegga Slide, offshore Norway. *Geo-Marine Letters*, **28**, 43–51, https://doi.org/10.1007/s00367-007-0088-9.

Roberts, J. J., and J. A. Tyburczy , 1994. Frequency-dependent electrical properties of minerals and partial melts. *Surveys in Geophysics*, **15**, 239–262, doi:10.1007/bf00689861.

Roberts, J. J., and J. A. Tyburczy, 1999. Partial-melt electrical conductivity: Influence of melt composition. *Journal of Geophysical Research-Solid Earth*, **104**, 7055–7065, doi:10.1029/1998jb900111.

Schwalenberg, K., M. Haeckel, J. Poort, and M. Jegen, 2010. Evaluation of gas hydrate deposits in an active seep area using marine controlled source electromagnetics: Results from Opouawe Bank, Hikurangi Margin, New Zealand. *Marine Geology,*, **272**, 89–98.

Stern, L. A., S. H. Kirby, S. Circone, and W. B. Durham, 2004. Scanning electron microscopy investigations of laboratory-grown gas clathrate hydrates formed from melting ice, and comparison to natural hydrates. *American Mineralogist*, **89**, 162–1175.

Stern, L.A., S.H. Kirby, and W.B. Durham, 1996. Peculiarities of methane clathrate hydrate formation and solid-state deformation, including possible superheating of water ice. *Science*, **273**, 1843–1848, doi:10.1126/science.273.5283.1843.

Wadhams, P., 2016. *A Farewell to Ice*. Penguin Random House, UK.

Wang, M., M. Deng, Z. L. Wu, X. H. Luo, J. N. Jing, and K. Chen, 2017. The deep-tow marine controlled-source electromagnetic transmitter system for gas hydrate exploration. *ournal of Applied Geophysics*, **137**, 138–144.

Weitemeyer, K.A., S.C. Constable, K.W. Key, and J.P. Behrens, 2006. First results from a marine controlled-source electromagnetic survey to detect gas hydrates offshore Oregon. *Geophysical Research Letters*, **33**, L03304, doi:10.1029/2005GL024896.

Yamamoto, K., Terao, Y., Fujii, T., Ikawa, T., Seki, M., Matsuzawa, M., and Kanno, T., 2014. Operational overview of the first offshore production test of methane hydrates in the Eastern Nankai Trough. Contributed paper at *Offshore Technology Conference, (OTC-25243-MS). https://doi.org/ 10.4043/25243-MS*, .

In-situ and laboratory evidence for high electrical anisotropy in marine gas hydrate

Steven Constable, Ryan Lu, Peter Kannberg, Laura Stern, Wyatt Du Frane and Jeffery Roberts

Marine gas hydrate is electrically resistive compared to the surrounding hydrate-free formation, a property that is exploited in borehole logging and also by marine controlled-source electromagnetic (CSEM) surveys. Well logging shows that hydrate can be electrically anisotropic, with vertical resistivities up to 10 times higher than horizontal resistivities, although the use of logging tools capable of measuring anisotropy is the exception rather than the rule. Marine CSEM methods are well known to be sensitive to anisotropy in seafloor sediments, and, for example, we have observed anisotropies of more than an order of magnitude using CSEM to map offshore relict permafrost.

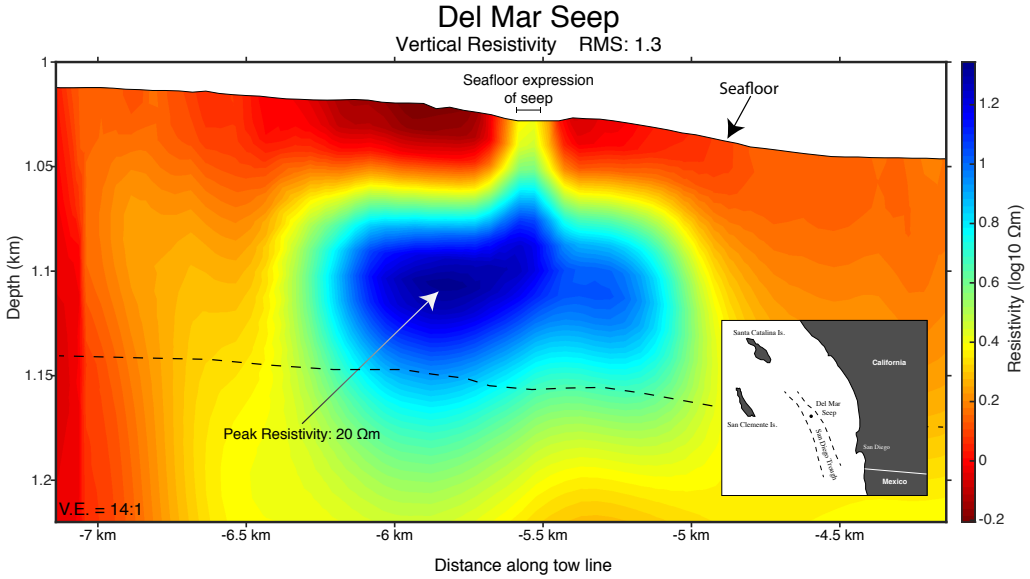

Figure 1. Vertical electrical resistivity model of the Del Mar Seep. Inset shows seep location, and broken line the inferred depth of the gas hydrate stability field. Note the large vertical exaggeration.

We have developed a deep-towed CSEM system for the purpose of imaging sub-seafloor gas hydrate, which we call Vulcan. The Vulcan system has been used in the Gulf of Mexico (see accompanying article), offshore Japan, and the North Atlantic. During a 2015 test of Vulcan in the San Diego Trough off southern California, we towed our CSEM system over the Del Mar Seep, a cold seep that intermittently vents methane in 1 km water depths. Inversion of the Vulcan data reveals a 100 m thick, 1,500 m diameter resistive feature, directly under the seep and within the gas hydrate stability field (Figure 1). We interpret this resistor to be gas hydrate formed from methane migrating to the surface along the San Diego Trough fault zone. Resistivities in the vertical direction peak at about 20 Ωm, large for in-situ CSEM measurements, suggesting high concentrations of hydrate.

An isotropic resistivity model cannot fit both the amplitude and phase of the electromagnetic data, and anisotropic inversion, in which the vertical resistivity varies from the horizontal resistivity, is required. While anisotropy ratios (vertical resistivity divided by horizontal resistivity) of 2–3 are common in marine sediments, under the seep anisotropy ratios are 20 or more (Figure 2). This is similar to what we have observed in offshore permafrost, but much larger than has been previously observed in seafloor gas hydrate using CSEM methods.

One model of anisotropy in gas hydrate consists of inter-bedded layers of water saturated sediment and gas hydrate, which has been used to explain anisotropy in borehole logs. It seems reasonable that hydrate forms preferentially in

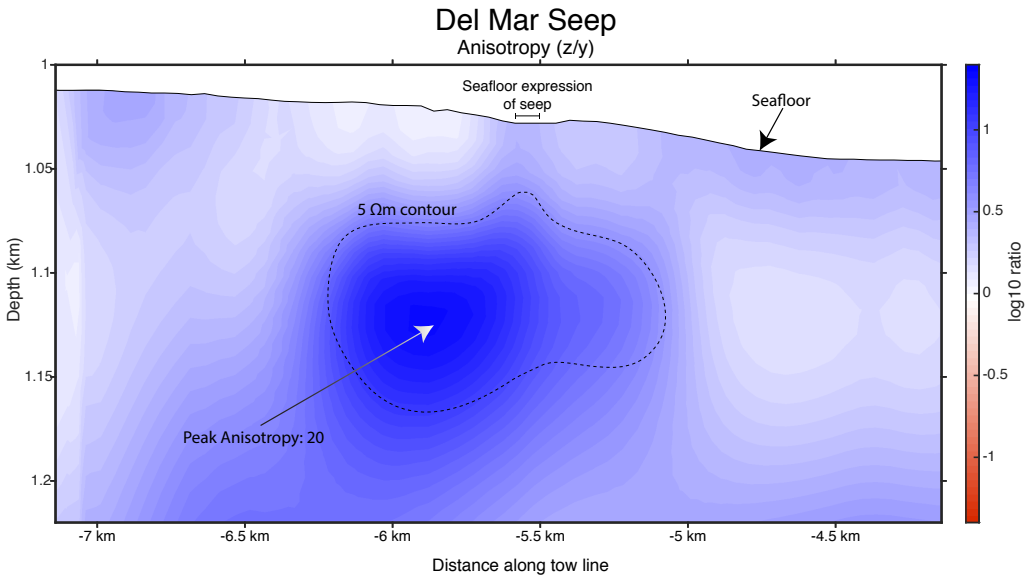

Figure 2. Ratio of vertical to horizontal resistivity for the Del Mar Seep model.

more permeable, coarser grained, layers. We recently carried out laboratory measurements on gas hydrate/sediment mixtures that adds nuance to this explanation (Figure 3). We mixed natural silica sediment of two different grain sizes (sand and silt) with either ice made from purified water, or ice made from flash-frozen seawater, and placed the mix in a pressure/temperature vessel. We synthesized ice to methane hydrate under high pressure methane by cycling the temperature back and forth across the ice solidus. After full synthesis, electrical resistivity was estimated using "impedance spectroscopy", in which both in-phase and out-of-phase sample resistance is measured over a range of frequencies, allowing the polarizing effect of the sample electrodes to be removed and to provide additional information about conduction mechanisms.

Sediment grain size has a small effect on electrical resistivity, and so grain size alone does not explain high anisotropies. As one would expect, samples with hydrate made from seawater are much less resistive than samples made from pure ice, about two orders of magnitude at 0°C. Although hydrate excludes salt during formation, our other studies suggest that the resistivity of the samples with hydrate made from pure ice is determined by a very small amount of salt, obtained from impurities on the sediment, being incorporated into the methane hydrate. For the seawater-hydrate sample, we infer that most of the salt is excluded and that resistivity is determined by a saturated brine phase mixed with resistive sediment and hydrate grains.

How does this relate to the "real-world" measurements from the seep? In an open system, where hydrate forms and resulting brine is removed from the vicinity, the resistivity of sediment saturated with hydrate might be similar to the ice-hydrate samples, a few thousand Ωm at 5°C, consistent with some borehole logs. However, if the system is closed, as our laboratory samples are, then resistivity will be much lower, perhaps similar to our seawater-hydrate samples (about 10 Ωm at 5°C). This suggests another interpretation of the high anisotropies seen in our field study: Perhaps the Del Mar Seep hydrate forms alternating layers of hydrate where salt from seawater is excluded, and layers where brines have accumulated in association with hydrate. Again, this may be dependent on grain size, which affects permeability and capillary forces, but may also be a result of brines inhibiting hydrate formation, similar to anisotropy in permafrost, where we infer that brines excluded during ice formation are interbedded with layers containing ice. Note that the resolution of the CSEM method is such that, in this case, layers thinner than 5–10 m thick would not be individually resolved, and so macro-anisotropy produces similar results to micro-anisotropy. The bulk resistivities of the Del Mar Seep model are lower than the laboratory measurements, but inevitably there will be some fraction of seawater (resistivity about 0.3 Ωm) in the system.

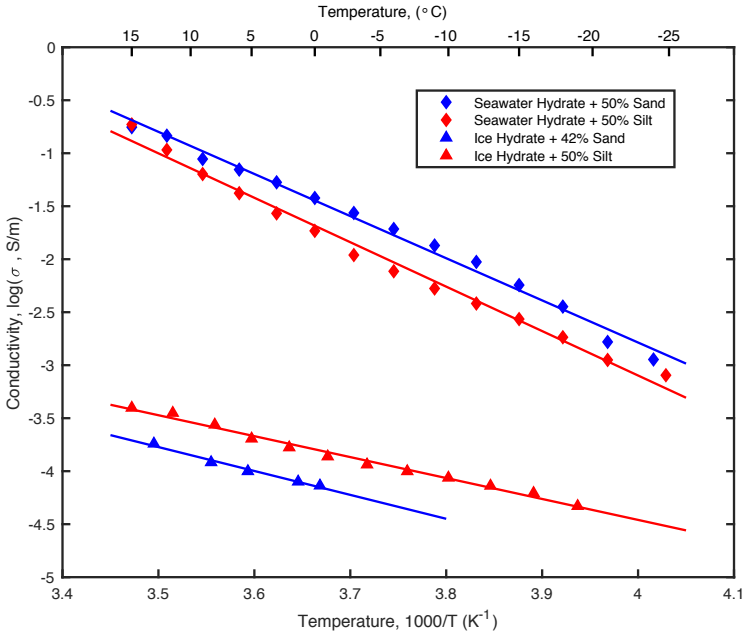

Figure 3. Laboratory measurements of electrical conductivity of silt (red) and sand (blue) mixed with methane hydrate synthesized from pure ice water (lower curves) and frozen seawater (upper curves).

Acknowledgements

We thank the captain and crew of the R/V New Horizon and John Pinkston for assistance with the field and laboratory work, respectively, and Bill Waite and Tom Lorenson for providing comments on a draft of the article. Laboratory work was supported by the US Department of Energy award DE-FE0028972 and DoE-USGS Interagency Agreement DE-FE0026382. Prepared by LLNL under Contract DE-AC52-07NA27344. Field data collection was supported by Ocean Floor Geophysics and the Scripps Seafloor Electromagnetic Methods Consortium.

SUGGESTED READING

Cook, A.E., B.I. Anderson, J. Rasmus, K.ıSun, Q. Li, T.S. Collett, D.S. Goldberg, 2011. Electrical anisotropy of gas hydrate-bearing sand reservoirs in the Gulf of Mexico. *Marine and Petroleum Geology*, **34**, 72–84, doi:10.1016/j.marpetgeo.2011.09.003.

Constable, S., P. K. Kannberg, and K. Weitemeyer, 2016. Vulcan: A deeptowed CSEM receiver. *Geochemistry, Geophysics, Geosystems*, **17**, 1042–1064, doi:10.1002/ 2015GC006174.

Lu, R., L.A. Stern, W.L. Du Frane, J.C. Pinkston, J.J. Roberts, and S. Constable, 2019. The effect of brine on the electrical properties of methane hydrate. *Journal of Geophysical Research: Solid Earth*, **124**, 10,877–10,892, doi:10.1029/2019JB018364.

Maloney, J.M., B.M. Grupe, A.L. Pasulka, K.S. Dawson, D.H. Case, C.A. Frieder, L.A. Levin, and N.W. Driscoll, 2015. Transpressional segment boundaries in strike-slip fault systems offshore southern California: Implications for fluid expulsion and cold seep habitats. *Geophysical Research Letters*, **42**, 4080–4088, doi = 10.1002/2015GL063778.

Sherman, D., and S.C. Constable, 2018. Permafrost extent on the Alaskan Beaufort Shelf from surface towed controlled-source electromagnetic surveys. *Journal of Geophysical Research: Solid Earth*, **123**, 1–13, /doi.org/ 10.1029/2018JB015859.

Gas hydrate characterization in the Gulf of Mexico using electromagnetic methods.

P. K. Kannberg and S. Constable

Electrical resistivity of sediments is commonly measured to identify formations containing methane hydrate, typically during borehole logging where higher resistivities indicate higher hydrate concentrations. However, inferring in situ resistivity using controlled source electromagnetic (CSEM) methods has also become a standard tool in hydrate exploration. In 2017 we collected 360 line kilometers of CSEM data on Walker Ridge 313, Orca Basin (WR100), Mad Dog (GC781), and Green Canyon 955 in the Gulf of Mexico, all areas with known or seismically inferred gas hydrate deposits and which have be drilled or targeted for future drilling. Here we present resistivity cross-sections obtained at WR313, Orca Basin, and GC955 (figure 1).

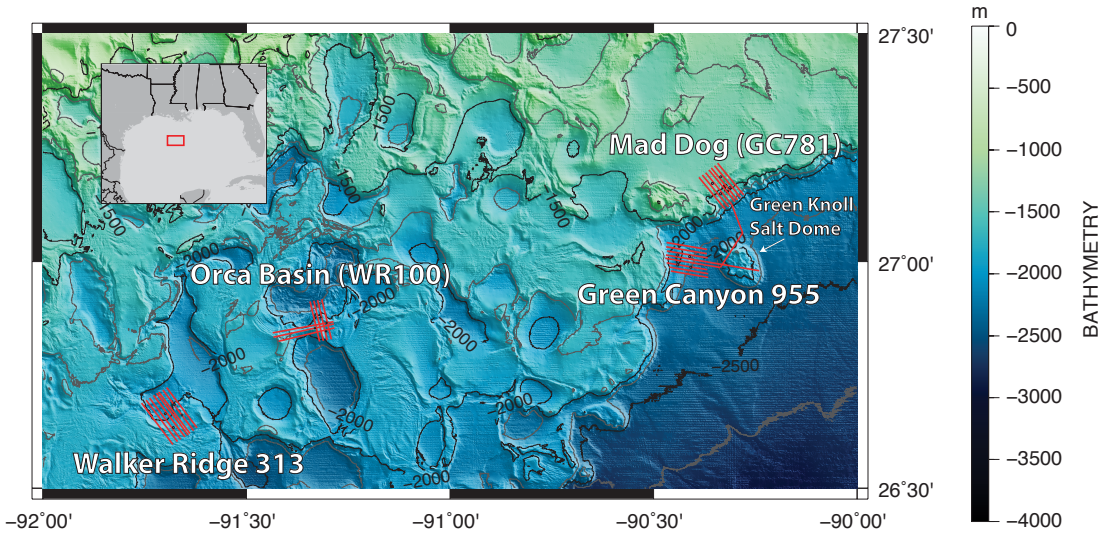

Figure 1: Map of the four survey areas. Inverted tow lines are marked as red lines on the map. Fence plots of the resistivity profiles are shown in figures 2, 3, and 4. Mad Dog (GC781) is not included in this manuscript.

We deep-towed an EM transmitter that generates an alternating electric field which propagates through the seafloor geology. Data were recorded on 6 receivers towed behind the transmitter at distances between 550 and 1550 m. In the presence of conductive geology, the electric fields will be attenuated, and conversely, in resistive geology the fields will be preserved. Our data were inverted using a 2D inversion method that first optimizes the model-data misfit, then finds the smoothest model fitting the data. This ensures that resistivity structures present in the final model are likely necessary.

At Walker Ridge 313, data were inverted along 8 parallel profiles (figure 2a). All inversions are anisotropic, where vertical resistivity can vary from horizontal resistivity. Salt tectonics at WR313 profoundly affects the structure of modeled resistivity. Salt bodies flank the basin on all sides, apparent as regions of high resistivity surrounded by a conductive halo, interpreted to be the result of increased pore fluid salinity and temperature adjacent to the salt bodies. Additionally, rising salt bodies control the local thrust faulting in the basin. When the resistivity models are overlain on seismic sections, increased resistivity is found in the unnamed unit that is bounded by the “aqua” and “yellow” sands (figure 2b). Within this unit, resistivity is further enhanced adjacent to faults, which appear to form a structural trap, with hydrate concentrating in these areas. We also see a less pronounced increase in resistivity at depths where we expected to find the base of the hydrate stability field, such as between kilometer 2-4 in WR313 line 5 (figure 2b).

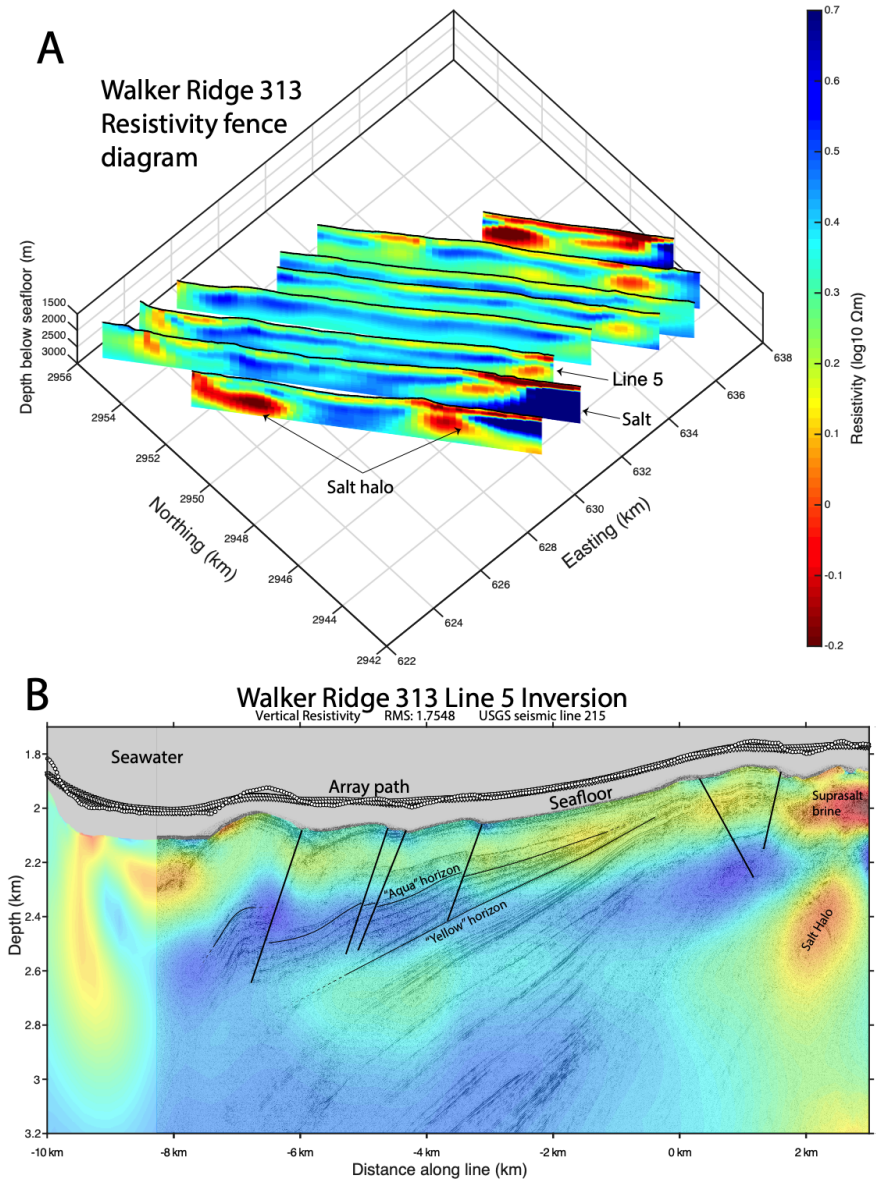

Figure 2: Walker Ridge 313 fence plot (A) showing resistivity cross sections as viewed from the southwest. All inversions shown here have blue colors as more resistive, and red colors as more conductive. The conductive brine halos surround the resistive salt bodies. A single line from the fence plot is overlain on the coincident seismic profile (B). Increased resistivity is strongest within the depths bounded by the "Aqua"and "Yellow" horizons and adjacent to faults.

These are collocated with sand beds thought to be hydrate-bearing and which were the target of the logging operations during the Gulf of Mexico Gas Hydrate Joint Industry Project Leg II (JIP). The resistivity values modeled from the real data are roughly the same as those in pre-survey synthetic inversions using logging resistivities from the JIP.

We analyzed CSEM inversions of seven lines across the ridge south of Orca Basin, including a slump feature on the western side of the ridge (figure 3a). Increased resistivities within the slump provide a correlative, though not causative, link between hydrate and slope failure in the Orca Basin. Historically, hydrate mediated slope failure was expected to occur at the base of the hydrate stability field (BHSF), where free gas causes overpressure, leading to slope failure

along the BHSF. Recent studies, using both modeling and observations, suggest an alternate mechanism of hydrate mediated slope failure which is caused by overpressurized sediments within the HSF. Such mechanisms manifest as a vertical pipe structure of hydrate or free gas that extends above the BHSF and terminates at an impermeable barrier, increasing pore pressures laterally along the base of the trap. One of our inversions across the Orca Basin slump (figure 2b) shows a dipping resistor that spreads laterally at the seafloor, possibly representing the relict hydrate plumbing system left behind after slope failure occurred. A slope failure mechanism such as this would be retrogressive, which is what is occurring at the Orca Basin slump.

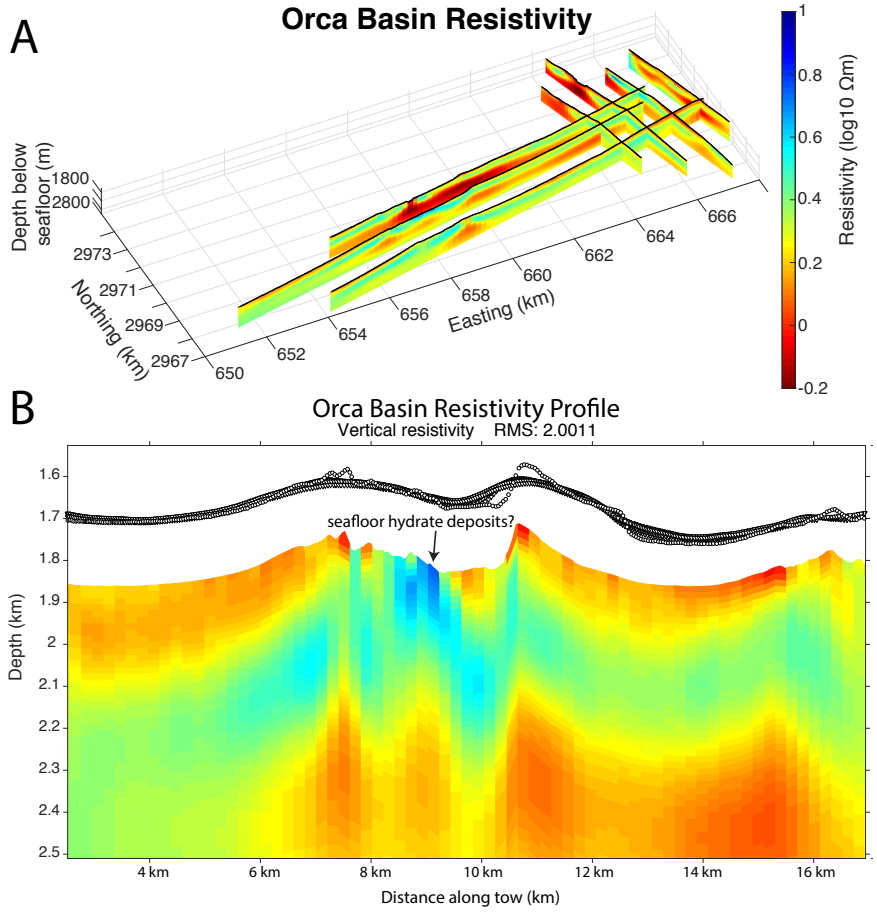

Figure 3: Orca Basin resistivity fence plot (A) and selected profile (B). The profile in B shows shallow hydrates that could be the remnants of a hydrate system that precipitated the slope failure within the slump.

Eight CSEM lines were towed at Green Canyon 955 (figure 4a). Well logs from GC955 are in rough agreement with our inversions, with GC955 hole H showing significant increased resistivity interpreted to be hydrate, while hole Q, located upslope, shows no increased resistivity (figure 4b). Below the hydrate bearing interval is another resistor that is coincident with the depth of seismically inferred free gas bearing sediments. Additionally, an area of increased resistivity between holes H and Q is coincident with a mud volcano and resembles that of methane seeps imaged around the world, where a broad, deep resistor is connected to the seafloor by a narrow resistive pipe.

In conclusion, at each of the proposed drilling sites we found increased resistivity, interpreted as increased hydrate concentrations. However, not only were the primary sites not always more resistive than the alternate sites, at WR313 the strongest resistors were not at the locations targeted for drilling.

Acknowledgements

This work was supported by the US Department of Energy award DE-FE0028972 and the Scripps Seafloor Electromagnetic Methods Consortium.

Recommended reading:

CSEM data acquisition system: Constable, S., Kannberg, P. K., and Weitemeyer, K., 2016, Vulcan: A deep-towed CSEM receiver, Geochem. Geophys. Geosyst., 17, 1042—1064. https://doi.org/10.1002/2015GC006174

Orca Basin Geology: Sawyer, D. E., Mason, R. A., Cook, A. E., & Portnov, A. 2019. Submarine Landslides Induce Massive Waves in Subsea Brine Pools. Nature - Scientific Reports, 128, 9, 1, 2045-2322. https://doi.org/10.1038/s41598-018-36781-7

Hydrate mediated slope failure: Elger, J., Berndt, C., Rcke, L., Krastel, S., Gross, F., & Geissler, W.H. 2018. Submarine slope failures due to pipe structure formation. Nature Communications. 9(1), 715, https://doi.org/10.1038/s41467-018-03176-1

Gulf of Mexico Gas Hydrate Joint Industry Project Leg II overview: Collett, T. S., Lee, M. W., Zyrianova, M. V., Mrozewski, S. A., Guerin, G., Cook, A. E., Goldberg, D. S. 2012. Gulf of Mexico Gas Hydrate Joint Industry Project Leg II logging-while-drilling data acquisition and analysis. Marine and Petroleum Geology, 34, 1, 41-61. https://doi.org/10.1016/j.marpetgeo

Other activities

Training and professional development.

Peter Kannberg, then a PhD student at SIO, acted as co-chief scientist on the data collection cruise. He is currently working on this project as a postdoc.

Ryan Lu, a junior scientist at LLNL, continues work on the laboratory electrical conductivity studies and learning about hydrate synthesis and the operation of the conductivity cell.

SIO PhD students Dallas Sherman and Valeria Reyes-Ortega participated in the research cruise and learnt about the operation of the CSEM instruments. Sherman assisted with an industry-operated hydrate survey later in that year.

Peter Kowalczyk and Karen Weitemeyer, of Ocean Floor Geophysics, participated in the cruise as part of the industry cost-share component, and also gained some training in the operation of the equipment, which has been used for several proprietary surveys offshore Japan.

Plans for next project period.

This concludes this project, so there is no future project period and no carry-over funds. All project goals and milestones have been met.

Table 1: Milestone status report.

Milestone Title	Planned Completion Date	Actual Completion Date	Verification Method	Comments on progress
First set of conductivity runs	08/1/2017	08/1/2017	Internal review	completed
Field data collection	12/1/2017	06/12/2017	200 line km collected	completed
Second conductivity runs	12/30/2017	12/30/2017	Internal review	completed
Final set of conductivity runs	8/1/2018	8/1/2018	Internal review	completed
Field data inverted	12/1/2018	7/1/2019	2D inversions done	completed
Publications(s) submitted	9/1/2019	7/11/2019	At least 1 pub. submitted	completed
Publications(s) accepted	12/30/2019	9/25/2019	Publication accepted	completed

PRODUCTS

Project Management Plan. The revised Project Management Plan was accepted on 3 February 2017.

Project Web Page. http://marineemlab.ucsd.edu/Projects/GoMHydrate2017/index.html (check out the animated movie of the deep-two over Green Canyon at http://marineemlab.ucsd.edu/Projects/GoMHydrate2017/deeptowmovie.html)

Preliminary Cruise Report. http://marineemlab.ucsd.edu/Projects/GoMHydrate2017/CruiseReportReduced.pdf

Fire in the Ice article. Electrical Conductivity of Methane Hydrate with Pore Fluids: New Results from the Lab Ryan Lu, Laura A. Stern, Wyatt L. Du Frane, John C. Pinkston, and Steven Constable. Fire in the Ice, 18, 7–12.

AGU abstracts:

Kannberg, P., and S. Constable, 2017: Deep-towed CSEM survey of gas hydrates in the Gulf of Mexico. Contributed paper at the Fall AGU meeting, New Orleans.

Lu, R., L.A. Stern, W.L./ Du Frane, J.C. Pinkston, J.J. Roberts and S. Constable, 2018: Electrical characterization of methane hydrate with coexisting brine. Contributed paper at the Fall AGU meeting, Washington.

Kannberg, P., and S. Constable, 2018: Quantifying Methane Hydrate in the Gulf of Mexico Using Controlled Source Electromagnetic Methods. Contributed paper at the Fall AGU meeting, Washington.

Other abstracts:

Kannberg, P., and S. Constable, 2018, Detecting methane hydrate in the Gulf of Mexico using controlled source electromagnetic methods. Contributed poster at the Galveston Gordon Conference.

The following papers acknowledge this or past DoE funded research:

Lu, R., L.A. Stern, W.L. Du Frane, J.C. Pinkston, J.J. Roberts, and S. Constable, 2019. The effect of brine on the electrical properties of methane hydrate. *Journal of Geophysical Research: Solid Earth*, **124**, 10,877–10,892.

Sherman, D., and S.C. Constable, 2018. Permafrost extent on the Alaskan Beaufort Shelf from surface towed controlled-source electromagnetic surveys. *Journal of Geophysical Research: Solid Earth*, **123**, 1–13, /doi.org/ 10.1029/2018JB015859.

Weitemeyer, K., S. Constable, D. Shelander, and S. Haines, 2017. Mapping the resistivity structure of Walker Ridge 313 in the Gulf of Mexico using the marine CSEM method. *Marine and Petroleum Geology*, **88**, 1013–1031, /doi.org/10.1016/j.marpetgeo.2017.08.039.

Sherman, D., P. Kannberg, and S. Constable, 2017. Surface towed electromagnetic system for mapping of subsea Arctic permafrost. *Earth and Planetary Science Letters*, **460**, 97–104.

Constable, S., P. K. Kannberg, and K. Weitemeyer, 2016. Vulcan: A deeptowed CSEM receiver. *Geochemistry, Geophysics, Geosystems*, **17**, doi:10.1002/ 2015GC006174.

Du Frane, W., L.A. Stern, S. Constable, K.A. Weitemeyer, M.M. Smith, and J.J. Roberts, 2015. Electrical properties of methane hydrate + sediment mixtures. *Journal of Geophysical Research*, **120**, 4773–4787, doi:10.1002/2015JB011940.

Weitemeyer, K., and S. Constable, 2014. Navigating marine electromagnetic transmitters using dipole field geometry. *Geophysical Prospecting*, **62**, 573–593, doi: 10.1111/1365-2478.12092.

Du Frane, W.L., L.A. Stern, K.A. Weitemeyer, S. Constable, J.C. Pinkston, J.J. Roberts, 2011. Electrical properties of polycrystalline methane hydrate. *Geophysical Research Letters*, **38**, doi:10.1029/2011GL047243.

Weitemeyer, K.A., S. Constable, S. and A.M. Trehu, 2011. A marine electromagnetic survey to detect gas hydrate at Hydrate Ridge, Oregon. *Geophysical Journal International* , **187**, 45-62.

Weitemeyer, K., G. Gao, S. Constable, and D. Alumbaugh, 2010. The practical application of 2D inversion to marine controlled-source electromagnetic sounding. *Geophysics*, **75**, F199–F211.

Weitemeyer, K., and S. Constable, 2010. Mapping shallow geology and gas hydrate with marine CSEM surveys. *First Break*, **28**, 97–102.

PARTICIPANTS AND OTHER COLLABORATING ORGANIZATIONS

Name:	Steven Constable
Project Role:	PI
Nearest person month worked:	1
Contribution to project:	Management, scientific direction
Funding support:	Institutional matching funds
Foreign collaboration:	Yes
Country:	Canada
Travelled:	No

Name:	Peter Kannberg
Project Role:	PhD student/SIO
Nearest person month worked:	3
Contribution to project:	Data processing and inversion.
Funding support:	This project
Foreign collaboration:	Yes
Country:	Canada
Travelled:	No

Name:	Laura Stern
Project Role:	Scientist/USGS
Nearest person month worked:	1
Contribution to project:	Gas hydrate synthesis and conductivity measurements.
Funding support:	USGS
Foreign collaboration:	No

Name:	Wyatt DuFrane
Project Role:	Scientist/LLNL
Nearest person month worked:	1
Contribution to project:	Postdoc supervision/conductivity measurements.
Funding support:	This project
Foreign collaboration:	No

Name:	Ryan Lu
Project Role:	Junior Scientist/LLNL
Nearest person month worked:	1
Contribution to project:	Conductivity measurements.
Funding support:	This project
Foreign collaboration:	No

CHANGES/PROBLEMS

There are no changes or problems arising from this review period.

National Energy Technology Laboratory

626 Cochrans Mill Road
P.O. Box 10940
Pittsburgh, PA 15236-0940

3610 Collins Ferry Road
P.O. Box 880
Morgantown, WV 26507-0880

13131 Dairy Ashford Road, Suite 225
Sugar Land, TX 77478

1450 Queen Avenue SW
Albany, OR 97321-2198

Arctic Energy Office
420 L Street, Suite 305
Anchorage, AK 99501

Visit the NETL website at:
www.netl.doe.gov

Customer Service Line:
1-800-553-7681

NATIONAL ENERGY TECHNOLOGY LABORATORY

U.S. DEPARTMENT OF ENERGY | NATIONAL ENERGY TECHNOLOGY LABORATORY